Symmetry energy of strange quark matter and tidal deformability of strange quark stars*

Jian-Feng Xu (https://orcid.org/0000-0003-3821-025X),[1,2,†] Cheng-Jun Xia,[3,‡]
Zhen-Yan Lu (https://orcid.org/0000-0002-2629-3329),[4,§] Guang-Xiong Peng,[5,6,¶] and Ya-Peng Zhao[7]

[1]*College of Information Engineering, Suqian University, Suqian 223800, China*
[2]*School of Physics and Electrical Engineering, AnYang Normal University, Anyang 455000, China*
[3]*Center for Gravitation and Cosmology, College of Physical Science and Technology, Yangzhou University, Yangzhou 225009, China*
[4]*Hunan Provincial Key Laboratory of Intelligent Sensors and Advanced Sensor Materials, School of Physics and Electronics, Hunan University of Science and Technology, Xiangtan 411201, China*
[5]*School of Nuclear Science and Technology, University of Chinese Academy of Sciences, Beijing 100049, China*
[6]*Institute of High-Energy Physics, Chinese Academy of Sciences, Beijing 100049, China*
[7]*School of Mathematics and Physics, Henan Urban Construction University, Pingdingshan 467036, China*

Research performed during the past decade revealed an important role of symmetry energy in the equation of state (EOS) of strange quark matter (SQM). By introducing an isospin-dependent term into the quark mass scaling, the SQM stability window in the equivparticle model was studied. The results show that a sufficiently strong isospin dependence $C_{\rm I}$ can significantly widen the SQM region of absolute stability, yielding results that simultaneously satisfy the constraints of the astrophysical observations of PSR J1614-2230 with 1.928 ± 0.017 $M_\odot$ and tidal deformability $70 \leq \Lambda_{1.4} \leq 580$ measured in the event GW170817. With increasing $C_{\rm I}$, the difference between the u, d, and s quark fractions for the SQM in $\beta-$equilibrium becomes inconspicuous for $C > 0$, leading to small isospin asymmetry δ, and further resulting in similar EOS and structures of strange quark stars (SQSs). Moreover, unlike the behavior of the maximum mass of u–d QSs, which varies with $C_{\rm I}$ depending on the sign of the parameter C, the maximum mass of the SQSs decreases monotonously with increasing $C_{\rm I}$.

Keywords: Symmetry energy, Strange quark matter, Strange stars, Tidal deformability

I. INTRODUCTION

At sufficiently high baryon number densities, strange quark matter (SQM) [1–4] with deconfined u, d, and s quarks is expected to be the true ground state of quantum chromodynamics (QCD). Owing to its possible implications in many fields, e.g., nuclear physics, astrophysics, and cosmology, it has garnered significant attention in the last few decades. Theoretically, SQM is a system dominated mainly by strong interactions, which can be studied in detail using QCD. Unfortunately, owing to the well-known quark confinement phenomenon at relatively low Densities, which could be relevant to neutron-star interiors and quark stars, perturbative QCD calculations of SQM are not reliable [5]. In addition, although the ab initio lattice QCD calculations were very successful in the finite-temperature regime with a zero chemical potential (baryon number density), they still suffer from the famous intractable Fermion sign problem [6]. Therefore, researchers typically resort to phenomenological models, such as the density-dependent model [7–11], quark cluster model [12, 13], quasi-particle model [14–18], Nambu-Jona-Lasinio model [19], and so on. In Refs. [20, 21], strong magnetic field effect on the properties of SQM had been investigated, and numerous interesting results have been obtained in other studies [22–25].

To study the SQM properties using phenomenological models, one of the most important issues is determining reasonable values of the model parameters. Given the conjecture that SQM is absolutely stable, the most commonly used constraint is that, for SQM, the energy per baryon should be smaller than 930 MeV, while for the bulk u-d quark matter (u-d QM) it should be larger than 930 MeV. Moreover, significant progress has been made in the observations of global properties of compact objects, such as mass, radius, and tidal deformability. For example, the measurements of PSR J1614-2230 and PSR J0348+0432 several years ago precisely determined masses of 1.97 ± 0.04 $M_\odot$ [26] (a more precise mass measurement yielded 1.928 ± 0.017 $M_\odot$ [27] with a 68% credible level) and 2.01 ± 0.04 $M_\odot$ [28], respectively. In addition, the more recently measured gravitational mass of PSR J0740 + 6620 reached $2.14^{+0.20}_{-0.18}$ $M_\odot$ with 95.4% credibility, likely making it the the largest compact star observed up to date [29] (the updated result for PSR J0740 + 6620 is $2.08^{+0.07}_{-0.07}$ $M_\odot$ [30] with 68.3% credibility). Therefore, these observations of pulsar masses have been widely used to constrain the EOS of compact stars and the onset of the phase transition from hadronic matter to quark matter in hybrid stars [31, 32].

In addition, with the coming of multi-messenger observations of neutron stars, owing to the detection of gravitational waves for events GW170817 [33] and GW190814 [34], additional stringent constraints on the EOS of compact star matter have been appeared [35–37]. Specifically, it was determined that for GW190814, the newly discovered compact

* This work was supported by the National Natural Science Foundation of China (Nos. 12005005 and 11875052), the National SKA Program of China (No. 2020SKA0120300), the Hunan Provincial Nature Science Foundation of China (No. 2021JJ40188), and the Scientific Research Start-up Fund of Talent Introduction of Suqian University (No. Xiao2022XRC061).
† xujf@squ.edu.cn
‡ cjxia@yzu.edu.cn
§ luzhenyan@hnust.edu.cn
¶ gxpeng@ucas.ac.cn

binary merger possesses a secondary component with mass as large as 2.50−2.67 $M_\odot$ at the 90% credibility level. If it is confirmed to be a compact star, rather than a light black hole, it will be possible to rule out many EOSs. Moreover, this detection of gravitational waves for GW170817 offers a novel opportunity to directly probe the properties of matter under extreme conditions found in the interior of compact stars, yielding improved estimates of tidal deformability $\Lambda_{1.4} = 190^{+390}_{-120}$ [38]. This measurement of tidal deformability has been widely used for constraining the properties of compact star matter [39–46].

Recently, an interesting proposition was made, suggesting that, instead of the SQM, the u-d QM may be the true ground state of QCD [47]. According to this proposition, it has been found that the properties of the u-d QS are in accordance with various astrophysical observations [48], where quark symmetry energy effects are included in the EOS of the u-d QM. In practice, it has been found that symmetry energy plays an important role in determining the properties of isospin asymmetry matter [49–53]. For nuclear matter, although the symmetry energy behaviors have been well determined below and around the saturation density, it remains a big challenge to determine the density behaviors of the symmetry energy at suprasaturation densities, where phase transitions of strong interaction matter may occur, and various new forms of matter may appear. In fact, due to the different symmetry terms in different phases, isospin effects are rather significant [54]. In this study, considering the isospin effects of the SQM, we investigated the stability window and symmetry energy of SQM, and employed some of the constraints mentioned above in the equivparticle model [23] to examine whether the SQS properties are consistent with the reported astrophysical observations. It is found that inter-quark isospin effects are necessary for reconciling the SQSs obtained in the equivparticle model with the aforementioned constraints.

The remainder of this paper is organized as follows. Section II A briefly describes the equivparticle model, where quark mass scaling with isospin effects is introduced. Then in Sect. II B, the equations for calculating the tidal deformability of compact stars are presented. In Sect. III, the numerical results of the properties of SQM and the structures of SQSs are given and discussed. Finally, we conclude this paper with a brief summary in Sect. IV.

II. EQUATIONS FOR SYMMETRY ENERGY AND TIDAL DEFORMABILITY

A. Equivparticle model with isospin asymmetry

In the equivparticle model, by introducing an effective quark chemical potential μ_i^*, the thermodynamic potential density of the quark matter system can be written as [23]

$$\Omega_0(\mu_i^*, m_i) = -\sum_i \frac{g_i m_i^4}{24\pi^2} f\left(\frac{\mu_i^*}{m_i}\right),$$

where $f(x) = x\sqrt{x^2-1}(x^2-\frac{5}{2}) + \frac{3}{2}\mathrm{arch}(x)$, g_i(=6 for quarks and 2 for electrons) is the particle degeneracy, m_i is the isospin density-dependent equivalent quark mass, and $\nu_i = \sqrt{\mu_i^{*2} - m_i^2}$ is the Fermi momentum of particle species i. Using the basic thermodynamic relation $\rho_i = -\mathrm{d}\Omega_0/\mathrm{d}\mu_i^*$, the particle number density ρ_i is readily obtained

$$\begin{aligned}\rho_i &= -\frac{\mathrm{d}\Omega_0}{\mathrm{d}\mu_i^*} = -\frac{\partial\Omega_0}{\partial\mu_i^*} - \frac{\partial\Omega_0}{\partial\nu_i}\frac{\partial\nu_i}{\partial\mu_i^*} = \frac{g_i\nu_i^3}{6\pi^2} \\ &= \frac{g_i}{6\pi^2}\left(\mu_i^{*2} - m_i^2\right)^{3/2}. \end{aligned} \quad (1)$$

Regarding the equivalent quark mass m_i, different types of quark mass scaling were constructed to account for strong inter-quark interactions [7, 10, 23, 55]. Conventionally, in the equivparticle model, m_i is a function of the baryon number density ρ_b. To include the isospin effect on the EOS of quark matter, the isospin asymmetry term $\delta \equiv 3(\rho_d - \rho_u)/(\rho_d + \rho_u)$ is introduced into the mass scaling framework. In Ref. [56], m_i is parameterized as $m_i(\rho_\mathrm{b}, \delta) = m_{i0} + D\rho_\mathrm{b}^{-1/3} - \tau_i\delta D_\mathrm{I}\rho_\mathrm{b}^{\alpha}\mathrm{e}^{-\beta n_\mathrm{b}}$ with τ_i being the third component of the isospin for quark flavor i. In this study, we used the parameterization that was recently proposed in Ref. [48], i.e.,

$$\begin{aligned} m_i(\rho_\mathrm{b}, \delta) &= m_{i0} + m_{\mathrm{I}i}(\rho_\mathrm{b}, \delta) \\ &= m_{i0} + D\rho_\mathrm{b}^{-1/3} + C\rho_\mathrm{b}^{1/3} + C_{\mathrm{I}i}\delta^2\rho_\mathrm{b}, \end{aligned} \quad (2)$$

where m_{i0} is the quark current mass, D is the confinement parameter indicating the linear confinement effect, C represents the one-gluon exchange interaction for $C < 0$ and the leading-order perturbative interaction for $C > 0$, and parameter $C_{\mathrm{I}i}$ ($C_{\mathrm{I}u} = C_{\mathrm{I}d}, C_{\mathrm{I}s} = 0$) is used for adjusting the strength of the isospin-dependent equivalent quark mass and thus the magnitude of the quark-matter symmetry energy. In addition, this equivalent quark mass satisfies the exchange symmetry between u and d quarks in quark matter in the absence of inter-quark electromagnetic interactions.

The energy density and pressure of the SQM are, respectively, given as

$$E = \Omega_0 - \sum_i \mu_i^* \frac{\partial\Omega_0}{\partial\mu_i^*} = \sum_i \frac{g_i m_i^4}{16\pi^2} g\left(\frac{\mu_i^*}{m_i}\right) \quad (3)$$

where $g(x) = x\sqrt{x^2-1}(2x^2-1) - \mathrm{arch}(x)$ and

$$P = -\Omega_0 + \rho_\mathrm{b}\sum_j \frac{\partial\Omega_0}{\partial m_j}\frac{\partial m_\mathrm{j}}{\partial\rho_\mathrm{b}} + \sum_{i,j}\rho_i\frac{\partial\delta}{\partial\rho_i}\frac{\partial\Omega_0}{\partial m_j}\frac{\partial m_\mathrm{j}}{\partial\delta}. \quad (4)$$

Based on the definition of the isospin asymmetry δ, the derivatives of δ with respect to ρ_u and ρ_d are, respectively

$$\frac{\partial\delta}{\partial\rho_u} = -\frac{6\rho_d}{(\rho_d+\rho_u)^2} \text{ and } \frac{\partial\delta}{\partial\rho_d} = \frac{6\rho_u}{(\rho_d+\rho_u)^2}. \quad (5)$$

Accordingly, the summation of the index i in the third term on the right-hand side of Eq. (4) is zero, which leads to the following simple pressure form:

$$P = -\Omega_0 + \rho_\mathrm{b}\sum_i \frac{\partial\Omega_0}{\partial m_i}\frac{\partial m_i}{\partial\rho_\mathrm{b}}, \quad (6)$$

with

$$\frac{\partial m_i}{\partial \rho_{\rm b}} = -\frac{D}{3{\rho_{\rm b}}^{4/3}} + \frac{C}{3{\rho_{\rm b}}^{2/3}} + C_{{\rm I}i}\delta^2, \tag{7}$$

and

$$\frac{\partial \Omega_0}{\partial m_i} = \frac{g_i m_i}{4\pi^2}\left[\mu_i^*\nu_i - m_i^2 \ln\left(\frac{\mu_i^*+\nu_i}{m_i}\right)\right]. \tag{8}$$

To obtain the EOS of the SQM, one has to solve the following equations, which are respectively the electric-charge neutrality conditions

$$2\rho_u - \rho_d - \rho_s - 3\rho_e = 0, \tag{9}$$

the conservation of the baryon number density

$$\rho_{\rm b} = \frac{1}{3}(\rho_u + \rho_d + \rho_s), \tag{10}$$

and the β-equilibrium condition

$$\mu_u + \mu_e = \mu_d = \mu_s. \tag{11}$$

It should be noted that the chemical potentials in Eq. (11) are real ones, instead of the effective ones. The relationship between the real chemical potential μ_i and effective chemical potential μ_i^* in the equivparticle model is

$$\begin{aligned}\mu_i &= \mu_i^* + \sum_j \frac{\partial \Omega_0}{\partial m_j}\frac{\partial m_j}{\partial \rho_i} \\ &= \mu_i^* + \frac{1}{3}\sum_j \frac{\partial \Omega_0}{\partial m_j}\frac{\partial m_j}{\partial \rho_{\rm b}} + \frac{\partial \delta}{\partial \rho_i}\sum_j \frac{\partial \Omega_0}{\partial m_j}\frac{\partial m_j}{\partial \delta},\end{aligned} \tag{12}$$

with

$$\frac{\partial m_j}{\partial \delta} = 2C_{Ij}\delta\rho_{\rm b}. \tag{13}$$

Using Eq. (12), Eq. (11) can be rewritten as

$$\mu_s^* = \mu_u^* + \frac{\partial \delta}{\partial \rho_u}\sum_j \frac{\partial \Omega_0}{\partial m_j}\frac{\partial m_j}{\partial \delta} + \mu_e, \tag{14}$$

and

$$\mu_s^* = \mu_d^* + \frac{\partial \delta}{\partial \rho_d}\sum_j \frac{\partial \Omega_0}{\partial m_j}\frac{\partial m_j}{\partial \delta}. \tag{15}$$

Using Eqs. (9) and (10), Eqns. (14) and (15) can be considered as a set of equations for ρ_u and ρ_d. By solving these equations for a given $\rho_{\rm b}$, we obtain ρ_u and ρ_d, and then, accordingly, the EOS of the SQM.

There are two methods for obtaining the symmetry energy. The first approach uses the parabolic law, approximately given by [56, 57]

$$E_{\rm sym}(\rho_{\rm b},\rho_s) \simeq \frac{1}{9}[E(\rho_{\rm b},\delta=3,\rho_s) - E(\rho_{\rm b},\delta=0,\rho_s)], \tag{16}$$

which implies that the symmetry energy is an estimate of the energy cost required for converting all u quarks in the symmetric u-d QM to d quarks, for given $\rho_{\rm b}$ and ρ_s. The other one can be analytically deduced from the following definition, i.e.,

$$E_{\rm sym}(\rho_{\rm b},\rho_s) = \frac{1}{2}\frac{\partial^2 E_{uds}/\rho_{\rm b}}{\partial \delta^2}\bigg|_{\delta=0}, \tag{17}$$

where

$$\begin{aligned}E_{uds} &= \frac{g}{2\pi^2}\int_0^{(1-\delta/3)^{\frac{1}{3}}\nu}\sqrt{k^2+m_u^2}k^2{\rm d}k \\ &+\frac{g}{2\pi^2}\int_0^{(1+\delta/3)^{\frac{1}{3}}\nu}\sqrt{k^2+m_d^2}k^2{\rm d}k \\ &+\frac{g}{2\pi^2}\int_0^{\nu_s}\sqrt{k^2+m_s^2}k^2{\rm d}k.\end{aligned} \tag{18}$$

Here, the Fermi momenta of u and d quarks are expressed, respectively, as

$$\begin{aligned}\nu_u &= (1-\delta/3)^{\frac{1}{3}}\nu, \\ \nu_d &= (1+\delta/3)^{\frac{1}{3}}\nu,\end{aligned} \tag{19}$$

where ν is the quark Fermi momentum of the symmetric u-d QM at the quark number density. $\rho = 2\rho_u = 2\rho_d$.

According to Eq. (18), Eq. (17) can be explicitly written as

$$\begin{aligned}&E_{\rm sym}(\rho_{\rm b},\rho_s) = \\ &\left(\frac{9C_I\rho_{\rm b}m}{2\nu^3}A + \frac{1}{18}\frac{\nu^2}{\sqrt{\nu^2+m^2}}\right)\frac{3\rho_{\rm b}-\rho_s}{3\rho_{\rm b}},\end{aligned} \tag{20}$$

with

$$A = \nu\sqrt{\nu^2+m^2} - m^2{\rm arcsh}\left(\frac{\nu}{m}\right), \tag{21}$$

where $m = m_0 + D\rho_{\rm b}^{-1/3} + C_{Ii}\rho_b^{1/3}$ with $m_0 \equiv m_{u0} = m_{d0}$. Here, we have assumed $m_{u0} = m_{d0}$. If $m_{u0} \neq m_{d0}$, then

$$\begin{aligned}&E_{\rm sym}(\rho_{\rm b},\rho_s) = \\ &\left(\frac{3C_{\rm I}\rho_{\rm b}m'_u}{2\nu^3}A_u + \frac{1}{54}\frac{\nu^2}{\sqrt{\nu^2+m_u'^2}}\right)\frac{3\rho_{\rm b}-\rho_s}{2\rho_{\rm b}} + \\ &\left(\frac{3C_{\rm I}\rho_{\rm b}m'_d}{2\nu^3}A_d + \frac{1}{54}\frac{\nu^2}{\sqrt{\nu^2+m_d'^2}}\right)\frac{3\rho_{\rm b}-\rho_s}{2\rho_{\rm b}},\end{aligned} \tag{22}$$

with

$$m'_i = m_{i0} + D\rho_{\rm b}^{-1/3} + C_{{\rm I}i}\rho_{\rm b}^{1/3} \tag{23}$$

and

$$A_i = \nu\sqrt{\nu^2+m_i'^2} - m_i'^2{\rm arcsinh}\left(\frac{\nu}{m'_i}\right). \tag{24}$$

We found that the discrepancy between the symmetry energies given by Eq. (20) and Eq. (22) is essentially negligible. Therefore, in the following calculations, we adopted Eq. (20) to calculate the SQM symmetry energy.

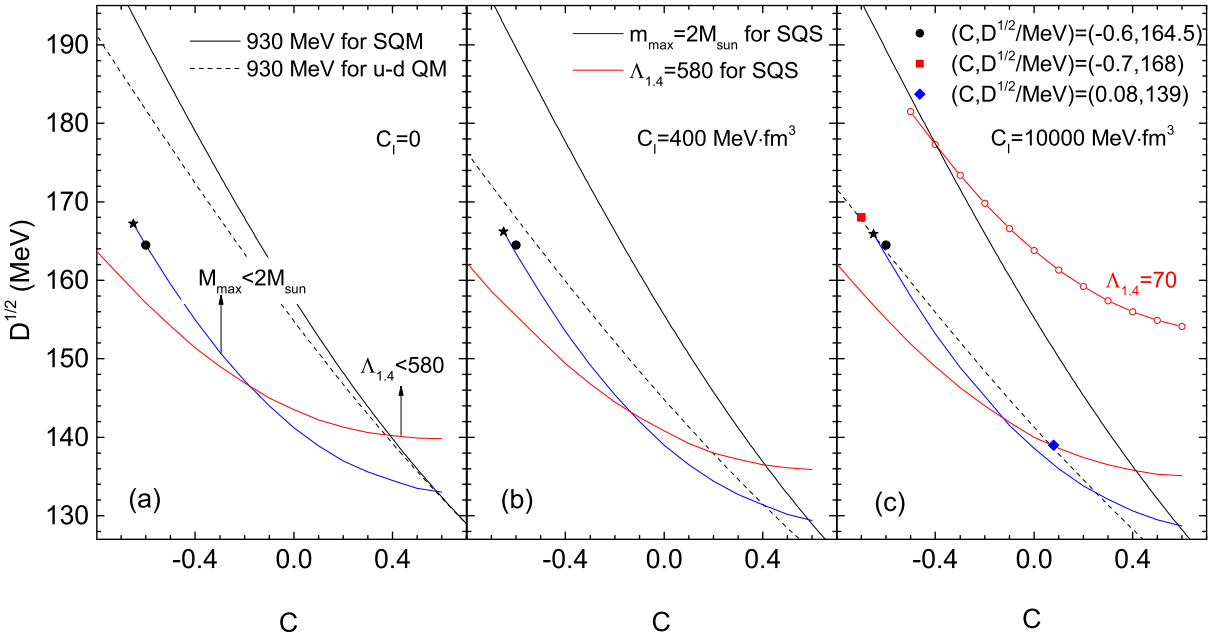

Fig. 1. (Color online) Stability windows for the SQM, for different values of the isospin strength parameter $C_{\rm I}$. The absolute-stability region between the black solid and dashed lines widens significantly with increasing $C_{\rm I}$, yielding results consistent with both the astrophysical observations of massive compact star PSR J1614-2230 with $1.928 \pm 0.017\ M_\odot$ and tidal deformability $70 \leq \Lambda_{1.4} \leq 580$, measured for GW170817. The blue line denotes the maximum mass of the SQSs with $2\ M_\odot$, the red line represents the upper limit of tidal deformability measured for GW170817, i.e., $\Lambda_{1.4} = 580$, and the red line with circles in panel (c) gives the lower limit $\Lambda_{1.4} = 70$. The typical model parameters are indicated in panels.

B. Equations for calculating structures and tidal deformability of SQSs

To calculate the structures and tidal deformability of SQSs, we briefly introduce relevant equations. To obtain the SQS structures, one should numerically solve the Tolman-Oppenheimer-Volkov (TOV) equation:

$$\frac{\mathrm{d}P}{\mathrm{d}r} = -\frac{GmE}{r^2}\frac{(1+P/E)\left(1+4\pi r^3 P/m\right)}{1-2Gm/r}, \tag{25}$$

with subsidiary conditions:

$$\frac{\mathrm{d}m}{\mathrm{d}r} = 4\pi r^2 E, \tag{26}$$

where $G = 6.707 \times 10^{-45}\mathrm{MeV}^{-2}$ denotes the gravitational constant.

Dimensionless tidal deformability is defined as [58–61]

$$\Lambda \equiv \frac{2}{3}k_2 C^{-5}, \tag{27}$$

where $C \equiv \frac{M}{R}G$ is the compactness and k_2 is the gravitational Love number with its value usually in the range of 0.2–0.3. To calculate Λ as a function of the star mass M or radius R, we need the value of k_2, which is defined as

$$\begin{aligned} k_2 = {} & \frac{8C^5}{5}(1-2C)^2\left[2+2C\left(y_{\rm R}-1\right)-y_{\rm R}\right] \\ & \times\left\{2C\left[6-3y_{\rm R}+3C\left(5y_{\rm R}-8\right)\right]+4C^3\right. \\ & \times\left[13-11y_{\rm R}+C\left(3y_{\rm R}-2\right)+2C^2\left(1+y_{\rm R}\right)\right] \\ & \left.+3(1-2C)^2\left[2-y_{\rm R}+2C\left(y_{\rm R}-1\right)\right]\right. \\ & \left.\ln(1-2C)\right\}^{-1}, \end{aligned} \tag{28}$$

where $y_{\rm R} \equiv y(R)$ and $y(r)$ is obtained as the solution to the following differential equation:

$$r\frac{\mathrm{d}y}{\mathrm{d}r} + y^2 + yF(r) + r^2 Q(r) = 0. \tag{29}$$

Here, $F(r)$ and $Q(r)$ are, respectively, defined as

$$F(r) \equiv \frac{1-4\pi r^2[\epsilon(r)-P(r)]G}{f(r)}, \tag{30}$$

and

$$\begin{aligned} Q(r) \equiv & \frac{4\pi}{f(r)}\left[5\epsilon(r)G + 9P(r)G + \frac{\epsilon(r)+P(r)}{v_s^2(r)}G\right. \\ & \left.-\frac{6}{4\pi r^2}\right] - 4\left[\frac{m(r)+4\pi r^3 P(r)}{r^2 f(r)}G\right]^2, \end{aligned} \tag{31}$$

where $v_s^2 = \partial P(r)/\partial\epsilon(r)$ denotes the squared sound velocity. In the case of a bare SQS, the energy density on the star

surface is finite, which requires a correction to be added to the calculation of $y_{\rm R}$ to account for the energy discontinuity, reading

$$y_{\rm R} \to y_{\rm R} - \frac{4\pi R^3 \epsilon_{\rm s}}{M}, \tag{32}$$

where $\epsilon_{\rm s}$ is the energy density difference between internal and external regions.

III. NUMERICAL RESULTS AND DISCUSSION

To study the isospin effects on the EOS of the SQM and the SQS structures, the values of the model parameters should be designated. First, the current masses of quarks are given as $m_{u0} = 5$ MeV, $m_{d0} = 10$ MeV, and $m_{s0} = 100$ MeV. If Eq. (20) is used for computing the symmetry energy, the values of the up and down quark current masses are $m_{u0} = m_{d0} = 7.5$ MeV. The values of the parameters C, D, and $C_{\rm I}$ are determined by studying the SQM stability window, combined with the astrophysical observation data of both massive compact star PSR J1614-2230 with $1.97\pm0.04\ M_\odot$ and tidal deformability $70 \leq \Lambda_{1.4} \leq 580$ measured for GW170817.

Shown in Fig. 1 are the SQM stability windows for different $C_{\rm I}$, with the value labeled in each panel. The black solid line in each panel indicates 930 MeV per baryon for the SQM; the SQM becomes unstable if the energy per baryon exceeds 930 MeV. Similarly, the dashed line in each panel corresponds to the 930 MeV (per baryon) level for the u-d QM; below this level, the energy per baryon of the bulk u-d QM is smaller than 930 MeV, and nuclei are likely to decay to the u-d QM. This case contradicts the modern nuclear physics and should be forbidden. Therefore, only the area between the black solid and dashed lines is the SQM's absolute-stability region. In addition, the blue line in each panel represents the configuration that can yield the maximum SQS mass with 2 $M_\odot$. However, when $C_{\rm I}$ and/or C are negative, and baryon number density is sufficiently large, further decreasing $C_{\rm I}$ will lead to a negative quark mass and the requirement of maximum mass with 2 $M_\odot$ will be no longer satisfied. Therefore, the blue lines in Fig. 1 will end at a certain point that is indicated by a star. The red line indicates the upper limit of $\Lambda_{1.4} = 580$ measured for GW170817. Moreover, it is worth mentioning that, if we decrease the values of the maximum mass $M_{\rm max}$ or tidal deformability $\Lambda_{1.4}$, the lines representing them will shift upward, as indicated in panel (a) with up arrows.

Comparing the three panels in Fig. 1, it is evident that, by increasing the isospin dependence parameter, $C_{\rm I}$, the dashed line will move significantly downward, whereas the solid line will be barely affected. Consequently, this will widen the SQS stable region. However, comparing panels (b) and (c), it can be observed that, for sufficiently high isospin parameter $C_{\rm I}$ values (e.g., for $C_{\rm I} = 400$ MeV·fm^3), further increasing it does not affect the absolute-stability region. In particular, we verified that beyond $C_{\rm I} \gtrsim 10000$ MeV·fm^3, the absolute-stability region barely changed as the value of the parameter was further increased.

By contrast, the blue lines for massive SQSs with 2 $M_\odot$ and red lines for the SQS tidal deformability with $\Lambda_{1.4} = 580$ tend slightly downward as $C_{\rm I}$ increases, but neither is affected significantly by varying $C_{\rm I}$. To satisfy these two astrophysical observations (i.e., $M_{\rm max} = 2\ M_\odot$ and $\Lambda_{1.4} = 580$), the cross-points of the blue and red lines should be located in the absolute-stability region. Unfortunately, from these three panels, we can easily observe that, although the cross-point approaches the stable region with increasing $C_{\rm I}$, it does not end up in the stable region, even for $C_{\rm I}$ values as high as 10000 MeV·fm^3. Given that the absolute-stability region does not change significantly by increasing $C_{\rm I}$ when it is already sufficiently large, we conclude that in the equivparticle model with mass scaling as given by Eq. (2), the two observables $M_{\rm max} = 2\ M_\odot$ and $\Lambda_{1.4} = 580$ can not be simultaneously satisfied by one set of model parameters.

However, if we loosen the constraint on tidal deformability to its lower limit, namely decreasing $\Lambda_{1.4}$ to 70, the red line moves upward to the position of the red line with circles, as shown in panel (c). Therefore, it can be inferred that as $\Lambda_{1.4}$ decreases, the intersection point of the blue and red lines moves upward along the blue line. Therefore, we can choose the point $(C, D^{1/2}/{\rm MeV}) = (-0.6, 164.5)$ indicated by the black dot in panel (c) as one of the typical parameter sets, which is located in the SQM absolute-stability region. For comparison, we select parameter sets $(C, D^{1/2}/{\rm MeV}) = (-0.7, 168)$ and $(0.08, 139)$ as typical parameter sets for investigating the SQM properties and the SQS structures, which are respectively indicated with a red square and blue diamond in panel (c). To study the effect of isospins on the SQM properties and SQS structures, we also chose points $(C, D^{1/2}/{\rm MeV}) = (-0.6, 164.5)$ in panels (a) and (b) as typical model parameter sets indicated by black dots, which are in the SQM unstable region.

In Fig. 2, the density behavior of the energy per baryon is shown for typical parameters. The figure reveals that in the equivparticle model, the minimum energy (circles) for each curve is at exactly the same density as zero pressure (asterisks), satisfying the requirement of thermodynamic consistency. Moreover, the one-gluon exchange interaction ($C < 0$) can significantly lower the minimum energy per baryon, which makes SQM much more stable than normal nuclear matter. In addition, comparing the three black lines, we find that with increasing $C_{\rm I}$, the minimum energy per baryon increases. However, for high values of $C_{\rm I}$, the difference between the solid black line ($C_{\rm I} = 10000$ MeV·fm^3) and dashed black line ($C_{\rm I} = 400$ MeV· fm^3) becomes small. This is because, with increasing $C_{\rm I}$, the difference between u and d quark fractions becomes small in β-equilibrated SQM, which results in vanishing isospin asymmetry δ. We can examine this point in Fig. 3. With the parameter set $(C, D^{1/2}/{\rm MeV}) = (-0.6, 164.5)$, the quark fractions are expressed as different C_I values indicated in each panel in Fig. 3. Evidently, the differences between u, d and s quark fractions become smaller as $C_{\rm I}$ increases. In particular, for $C_{\rm I} = 10000$ MeV·fm^{-3}, the difference between the u and d quark fractions is small, which leads to vanishing δ. Additionally, in this case, it is interesting to note that when

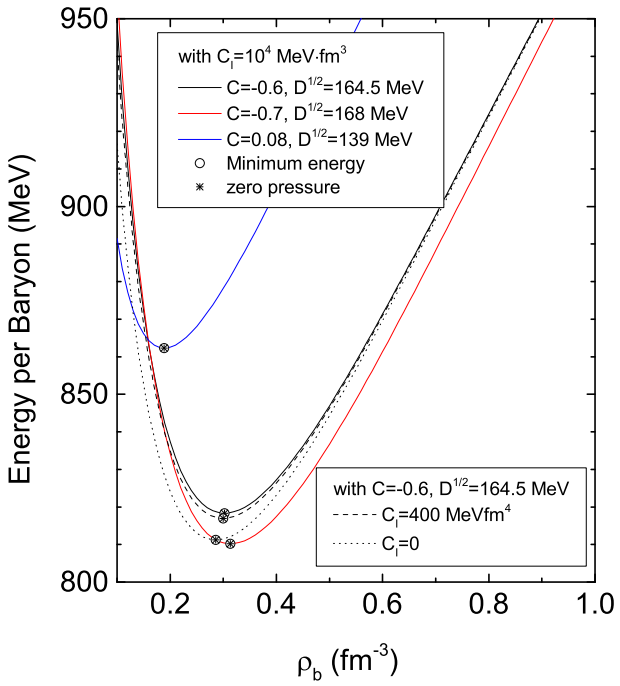

Fig. 2. (Color online) Density behavior of SQM energy per baryon in β-equilibrium. It is obvious that the minimal energy (circles) for each curve is exactly at the density corresponding to zero pressure (asterisks), satisfying the requirement of thermodynamic consistency.

$\rho_{\rm b} \gtrsim 0.6$ fm^{-3}, the u, d, and s quark fractions are essentially equal and approach 0.33, similar to the case of the color-flavor-locked (CFL) phase. The results for the density behavior of quark fractions in this study resemble those reported in Ref. [56].

Figure 4 shows the density behavior of the symmetry energy for typical parameters. From the left panel of Fig. 4, it can be seen that the value of C plays an important role in determining the symmetry energy. Generally, for the nuclear matter symmetry energy there are essentially two groups of density behavior, where one increases monotonously with density, and the other first increases and then decreases with increasing density [57, 62]. The latter is typically regarded as soft. Specifically, if the symmetry energy of nuclear matter becomes negative at suprasaturation densities, neutron stars exhibit pure neutron matter cores [63]. Similar to nuclear matter symmetry energy, the behavior of the SQM symmetry energy in the present work can be divided into two groups, depending on the value of the model parameter C. For non-negative C, the symmetry energy increases with increasing density. Otherwise, it first increases and then decreases with increasing density, which means that it becomes soft at high densities. However, unlike the nuclear matter symmetry energy, the quark matter symmetry energy in our model does not become negative, because the quark masses given by Eq. (2) become negative at sufficiently high densities with negative C. However, the soft quark matter symmetry energy will affect the chemical composition of the SQS core, and may have important implications for the structures and dynamical evolution of SQSs; this issue requires further studies.

Table 1. With the typical parameters $(C, D^{1/2}/\mathrm{MeV})$, the maximum mass $M_{\rm max}$, the radius corresponding to the maximum mass R, the central density n_0, and the quark matter symmetry energy at the SQS center $E_{\rm sym}$ are listed in the following table.

$(C, D^{1/2}/\mathrm{MeV})$	(0.08,139)	(-0.6,164.5)	(-0.7,168)
$M_{\rm max}/M_\odot$	1.93	1.97	2.01
R (km)	11.39	10.44	10.61
n_0 (fm^{-3})	0.98	1.20	1.11
$E_{\rm sym}$ (MeV)	7493.97	874.38	215.93

Moreover, as will be discussed later, to satisfy the requirement of the two-solar-mass constraint of the SQS maximum mass, the symmetry energies shown in the left panel can be as high as 3500 MeV, as indicated by the solid black line. In addition, in the left panel of Fig. 4 we also show the results from Fig. 1 in Ref. [56]; these are shown here by the red dashed line indicated with DI-300$\times$30. The reason for choosing the parameter set DI-300 for comparison was that the SQM symmetry energy with DI-300 is of the same order of magnitude as the nuclear matter symmetry given by the RMF model with interaction NL$\rho\delta$. Therefore, from this panel, we can see that the SQM symmetry energy is approximately 30 times higher than the nuclear matter symmetry energy, which is consistent with the findings in Ref. [56]. In addition, it is interesting to note that at relatively low densities, the symmetry energies shown by the black solid and dashed black lines are indistinguishable. The right panel of Fig. 4 shows that, on one hand, when $C_{\rm I} = 0$, the symmetry energy increases with increasing density, while when $C_{\rm I} = 400$ or 10000 MeV·fm^3, the symmetry energy first increases and then decreases for densities above 0.4 fm^{-3}; on the other hand, the symmetry energy increases drastically with increasing strength of the isospin dependence parameter $C_{\rm I}$, e.g., the symmetry energy for $C_{\rm I} = 10000$ MeV·fm^3 is approximately 20 times that for $C_{\rm I} = 400$ MeV·fm^3, or even more than 150 times that for vanishing $C_{\rm I}$.

Left and right panels of Fig. 5 show, respectively, the SQS structures and tidal deformability. The left panel of Fig. 5 shows that, as the isospin dependence parameter $C_{\rm I}$ increases, the maximum mass and the corresponding radius of the SQS decrease, which is different from some previously reported results [56]. Moreover, although all maximum mass values in the left panel are above 1.93 $M_\odot$, namely, the lower limit of the observed mass of PSR J1614-2230, only the black lines with parametric sets are in the SQM absolute-stability region, which is illustrated in Fig. 1. This finding reflects the crucial role of the symmetry energy on the SQM EOS in the equivparticle model. Typically, the black solid line with $(C, D^{1/2}/\mathrm{MeV}) = (-0.6, 164.5)$ and $C_{\rm I} = 10000$ MeV·fm^3 yields the maximum mass $M_{\rm max} = 1.97\ M_\odot$, corresponding to the measured mass of PSR J1614-2230. In addition, owing to the fact that with increasing SQS central density the quark equivalent mass given by Eq. (2) becomes negative, the dashed black line where $(C, D^{1/2}/\mathrm{MeV}) = (-0.7, 168)$

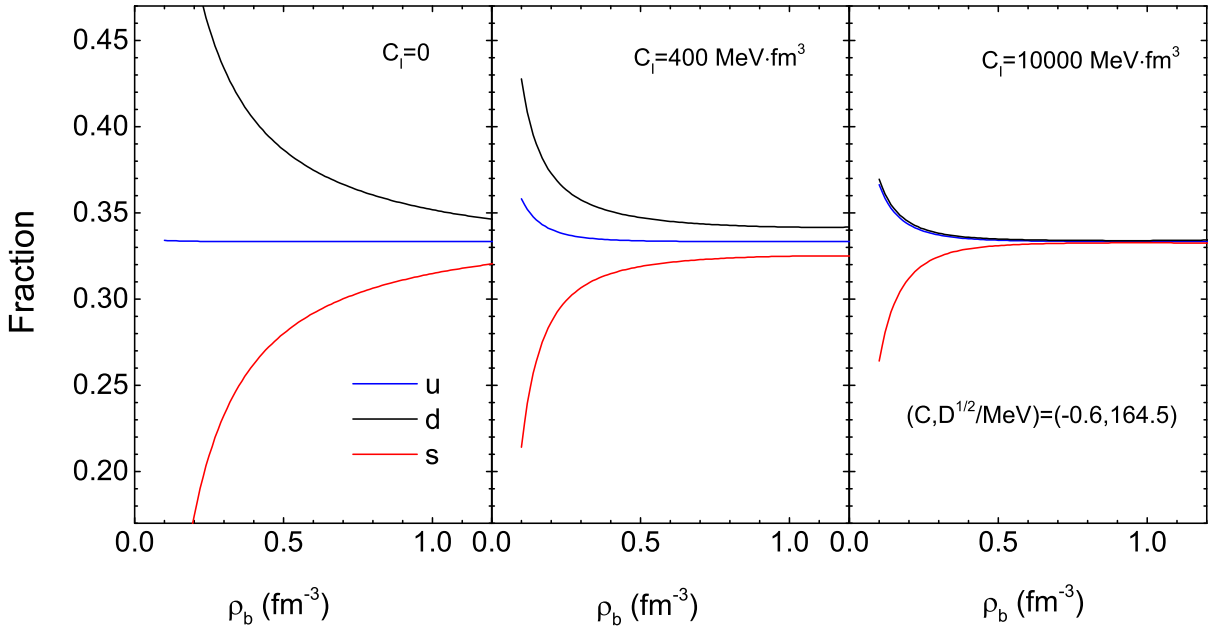

Fig. 3. Quark fraction as a function of the baryon number density in the equivparticle model, with the corresponding parameters indicated in each panel. The blue, black, and red lines are respectively for the u, d, and s quark fractions. See text for a detailed discussion.

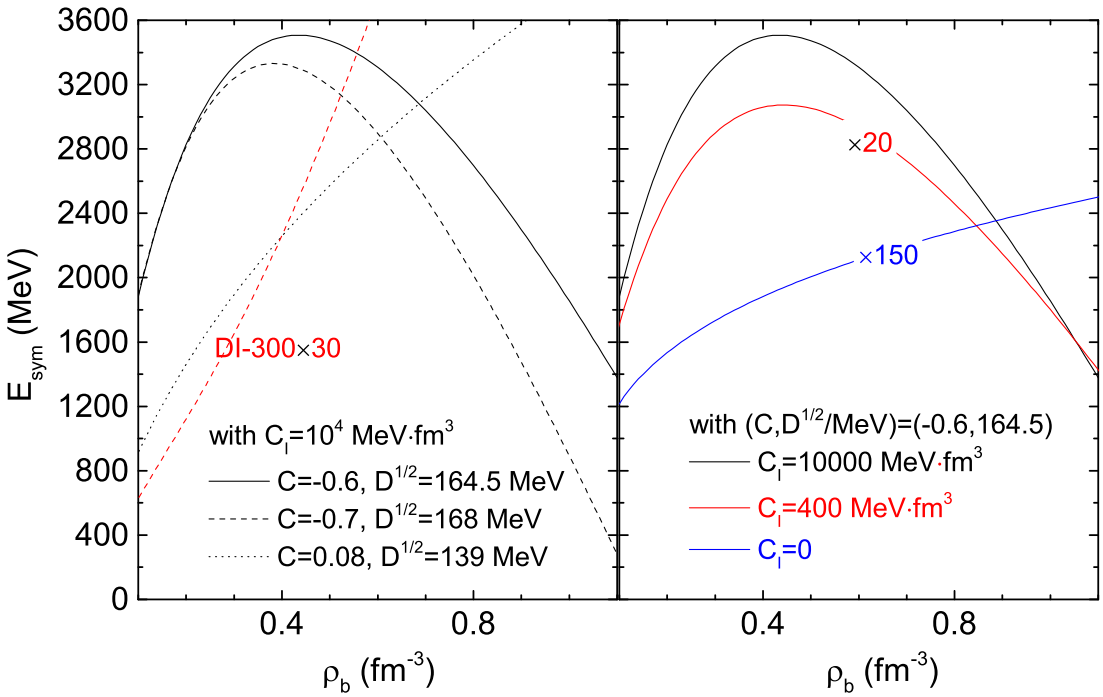

Fig. 4. Quark matter symmetry energy as a function of the baryon number density. The left panel shows that for $C < 0$ the symmetry energy peaks at a certain density. In addition, the red dashed line with DI-300 is replotted from Ref. [56], which has the same order of magnitude as nuclear matter symmetry energy. For the sake of comparison with the presently obtained results, we multiplied it by 30. Therefore, for satisfying the constraints imposed by astrophysical observations, the SQM symmetry energy can be as much as 30 times the nuclear matter symmetry energy. From the two panels we find that by increasing the isospin dependence parameter $C_{\rm I}$, the symmetry energy can be drastically increased, especially for $C > 0$.

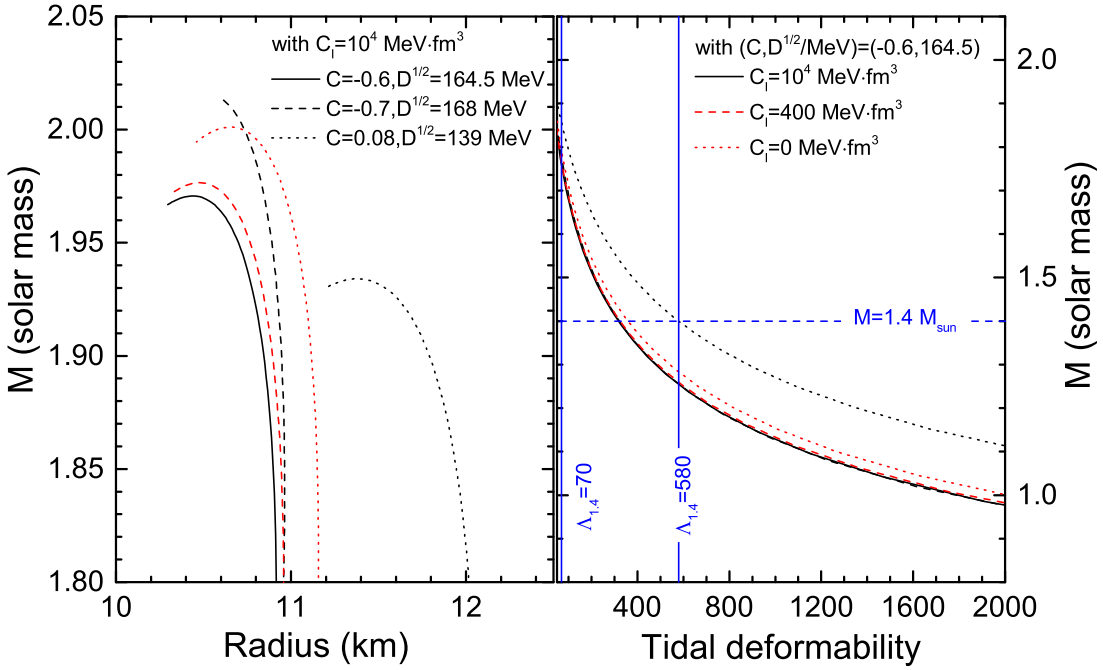

Fig. 5. Mass-radius relations of SQSs and the relation between the dimensionless tidal deformability and the SQS mass, for different model parameters. The solid black line for the parameter set $(C, D^{1/2}/\mathrm{MeV}) = (-0.6, 164.5)$ and $C_{\mathrm{I}} = 10000$ MeV·fm^{-3} yields the maximum mass $M_{\mathrm{max}} = 1.97\ M_{\odot}$, corresponding to the measured mass of PSR J1614-2230. Although the dashed black line does not reach the maximum mass for the configuration with the model parameter set $(C, D^{1/2}/\mathrm{MeV}) = (-0.7, 168)$ and $C_{\mathrm{I}} = 10000$ MeV·fm^{-3}, it yields the maximum mass above 2.01 $M_{\odot}$, which is in accordance with the observed mass of PSR J0348 + 0432.

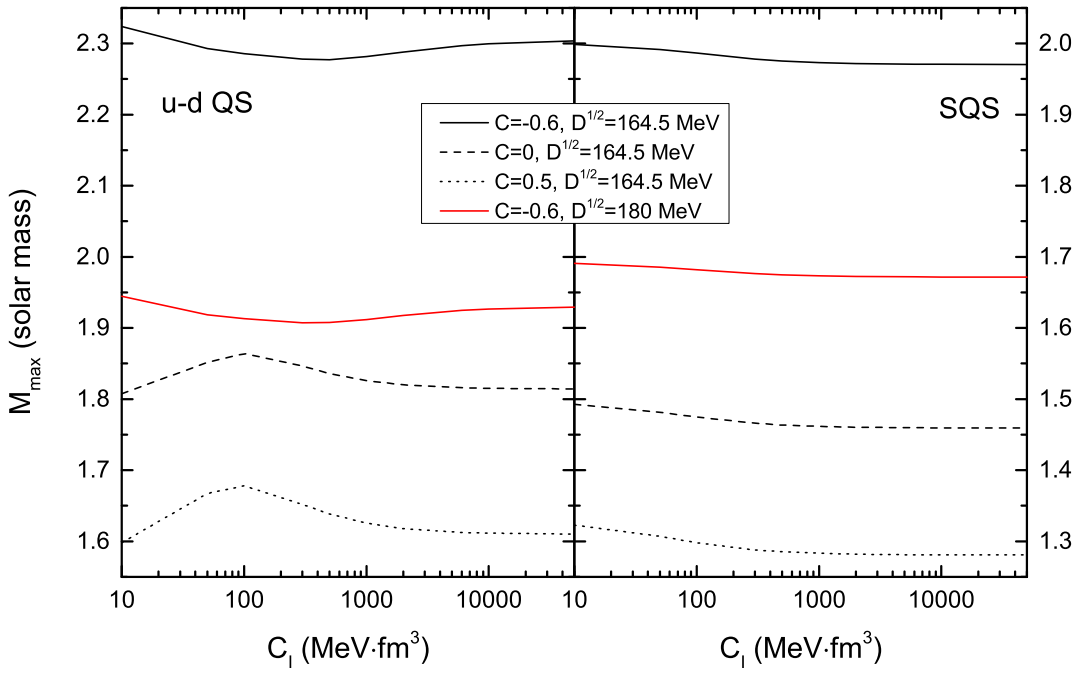

Fig. 6. Maximal SQS mass, as a function of C_{I}. Unlike the maximum SQS mass, which decreases monotonously with increasing C_{I}, the variation in the maximum mass of the u-d QS is complicated, depending on the sign of the model parameter C.

does not reach the maximum mass. However, the mass of the most massive star given by the black dashed line can exceed 2.01 $M_\odot$, which is in accordance with the measured mass of PSR J0348 + 0432 [28]. If we constrain the parameters to the SQM absolute-stability region in panel (c) of Fig. 1, we obtain that the SQS maximum mass can be as large as 2.02 $M_\odot$ in the present model, which is still within the limits of the measured mass of PSR J0740 + 6620 with values of 2.08 $\pm$ 0.07 $M_\odot$ [29]. Nevertheless, for GW190814 [34] it was shown that the binary merger possesses a secondary compact object with the mass as high as 2.50$-$2.67 $M_\odot$ at the 90% credibility level, which is far beyond the maximum mass of 2.02 $M_\odot$ in the present model. If the secondary compact object is a neutron star or a quark star, this may imply that other inter-quark interactions should be taken into consideration, or a novel quark mass scaling should be proposed for the equivparticle model. Specifically, Table I lists the typical quantities and symmetry energy for the SQS core. From Table 1, all the maximum masses shown are approximately 2 $M_\odot$, and with a positively valued model parameter C, the SQS maximum mass yields a lower central density. However, it is worth mentioning that the quark matter symmetry energy at the SQS center for positive C is much higher than that for negative C, although the central density is lower.

The right panel in Fig. 5 shows the relation between the dimensionless tidal deformability and the SQS mass, for the equivparticle model with different parameter sets in Fig. 5. The horizontal blue dashed line in the right panel of Fig. 5 corresponds to the SQS with 1.4 $M_\odot$, whereas the two blue solid lines indicate the range of the tidal deformability, that is, $70 \leq \Lambda \leq 580$, based on the improved analysis of GW170817 using LIGO and Virgo collaboration [38]. Note that the tidal deformability increases rapidly as the SQS mass decreases, which means that lighter SQSs can be deformed easier than heavier SQSs. Meanwhile, it is evident that all intersections of the typical lines and the blue dashed line are located between the two solid blue lines. Given the maximum masses in the left panel, the typical configurations with the parameter sets we have chosen in the present model can satisfy both the astrophysical observations of the massive compact star PSR J1614-2230 with 1.97 $\pm$ 0.04 $M_\odot$ and the tidal deformability $70 \leq \Lambda_{1.4} \leq 580$ measured for GW170817.

Shown in Fig. 6 is the dependence of the maximum mass on $C_{\rm I}$, for the u-d QS (left panel) and SQS (right panel). Comparing the two panels, it is evident that, for the same model parameters, the maximum u-d QS mass is higher than that of the SQS. In addition, unlike the maximum SQS mass, which decreases monotonously with increasing $C_{\rm I}$, the variation in the maximum mass of the u-d QS is complex. In particular, for nonnegative C the u-d QS maximum mass first increases with $C_{\rm I}$ at $C_{\rm I} < 100$ MeV·fm^3 and then decreases with $C_{\rm I}$; by contrast, for negative C the maximum u-d QS mass first decreases with increasing $C_{\rm I}$ to approximately 400 MeV·fm^3, and then increases with increasing $C_{\rm I}$. From these two panels, it is evident that for sufficiently large $C_{\rm I}$ (e.g., for $C_{\rm I} = 10000$ MeV·fm^3), further increasing $C_{\rm I}$ will not significantly affect the maximum mass. Furthermore, Fig. 6 shows that for $(C, \sqrt{D}/\mathrm{MeV})$ =(-0.6,164.5), the maximum u-d QS mass can be as large as 2.3 $M_\odot$, exceeding the observed 2.08 $M_\odot$ for J0740 + 6602. Nevertheless, in this case, the tidal deformability of the u-d QS yields $\Lambda_{1.4} \approx 720$, not in the $70 \leq \Lambda_{1.4} \leq 580$ range. This is illustrated in Table II, where the typical parameters $(C, D^{1/2}/\mathrm{MeV})$, the maximum mass $M_{\rm max}$, the tidal deformability $\Lambda_{1.4}$, and the energy per baryon $E/n_{\rm b}$ are shown for the u-d QS. Moreover, the data in the table suggest that, if the value of $\sqrt{D}$ is increased to 170, 175, or 180, the tidal deformability will be located in a reasonable range, but the maximum u-d QS mass will decrease as well. Specifically, for $(C, \sqrt{D}/\mathrm{MeV})$ =(-0.6,170), the energy per baryon for the u-d QM will exceed 930 MeV, implying an unstable state for the u-d QM, although the parameter set will yield proper values of $M_{\rm max} \approx 2.16 M_\odot$ and $\Lambda_{1.4} \approx 520$, satisfying the constraints of astrophysical observations. Therefore, for determining whether the u-d QS can simultaneously satisfy all of the above-mentioned constraints, further detailed investigations are needed.

Table 2. With the typical parameters $(C, D^{1/2}/\mathrm{MeV})$, for the u-d QS maximum mass $M_{\rm max}$, the tidal deformability $\Lambda_{1.4}$, and the energy per baryon $E/n_{\rm b}$ are listed in the following table, where $C_{\rm I} = 10^4$ MeV·fm^3.

$(C, D^{1/2}/\mathrm{MeV})$	(-0.6,164.5)	(-0.6,170)	(-0.6,175)	(-0.6,180)
$M_{\rm max}/M_\odot$	~2.30	~2.16	~2.04	~1.93
$\Lambda_{1.4}$	~720	~520	~380	~280
$E/n_{\rm b}$ (MeV)	~934	~965	~993	~1021

IV. SUMMARY

In this study, we investigated the isospin effects on the SQM stability window by introducing an isospin-dependent term into the quark mass scaling to account for the quark-matter symmetry energy, and further studied the EOS of the isospin-asymmetric SQM. We found that by increasing the isospin dependence parameter $C_{\rm I}$, the SQM absolute-stability region becomes significantly wider, therefore enabling support of the massive compact star PSR J1614-2230 with 1.97$\pm$ 0.04 $M_\odot$ and the tidal deformability $70 \leq \Lambda_{1.4} \leq 580$ measured for GW170817. As for quark fractions, we found that with increasing $C_{\rm I}$ the difference between u and d quark fractions became negligible, yielding vanishing isospin asymmetry δ; in addition, as the baryon number density increases, the u, d, and s quark fractions approach approximately 0.33, similar to the CFL phase results. The symmetry energy properties were then examined by considering different values of $C_{\rm I}$. It is interesting to note that for $C < 0$, with increasing $C_{\rm I}$ the SQM symmetry energy first increases and then decreases, implying soft symmetry energy. In addition, the symmetry energy increases drastically with increasing isospin dependence parameter $C_{\rm I}$, especially for $C > 0$. Owing to the widening of the SQM absolute-stability region by incorporating the isospin effects into the SQM EOS, the measured mass of PSR J1614-2230 with 1.97 $M_\odot$ and the dimensionless tidal deformability $70 \leq \Lambda_{1.4} \leq 580$ measured for GW170817 could

be well explained as SQSs by choosing proper model parameter values in the SQM absolute-stability region. However, considering that the measured mass of PSR J0740 + 6620 can be as large as 2.08 $M_\odot$, the present equivparticle model still cannot explain more massive SQSs with masses exceeding 2.02 $M_\odot$. This may imply that other SQM effects should be considered, e.g., the presence of u-d quark Cooper pairs (2SC phase) [51], or a novel quark mass scaling framework should be developed [56]. Finally, unlike the SQS maximum mass, which decreases monotonously with increasing $C_{\rm I}$, the variation in the u-d QS maximum mass is uncertain, depending on the sign of the model parameter C.

AUTHOR CONTRIBUTIONS

All authors contributed to the study conception and design. Material preparation, data collection and analysis were performed by Jian-Feng Xu, Cheng-Jun Xia,Zhen-Yan Lu,Guang-Xiong Peng and Ya-Peng Zhao. The first draft of the manuscript was written by Jian-Feng Xu and all authors commented on previous versions of the manuscript. All authors read and approved the final manuscript.

[1] A.R. Bodmer, Collaped nuclei. Phys. Rev. D **4**, 1601 (1971). doi:10.1103/PhysRevD.4.1601

[2] E. Witten, Cosmic separation of phases. Phys. Rev. D **30**, 272 (1984). doi:10.1103/PhysRevD.30.272

[3] H. Terazawa, Super-Hypernuclei in the Quark-Shell Model. J. Phys. Soc. Jpn. 58, 3555 (1989). doi:10.1143/JPSJ.58.3555

[4] E. Farhi, R.L. Jaffe, Strange matter. Phys. Rev. D 30, 2379 (1984). doi:10.1103/PhysRevD.30.2379

[5] K. Fukushima, T. Hatsuda, The phase diagram of dense QCD. Rept.Prog.Phys. **74**, 014001 (2011). doi:10.1088/0034-4885/74/1/014001

[6] I. Barbour, N.-E. Behilil, E. Dagotto, et al., Problems with finite density simulations of lattice QCD. Nucl. Phys. B **275**, 296 (1986). doi:10.1016/0550-3213(86)90601-2

[7] G. Fowler, S. Raha, R. Weiner, Confinement and Phase Transitions. Z. Phys. C **9**, 271 (1981). doi:10.1007/BF01410668

[8] S. Chakrabarty, S. Raha, B. Sinha, Strange quark matter and the mechanism of confinement. Phys. Lett. B **229**, 112 (1989). doi:10.1016/0370-2693(89)90166-4

[9] O. Benvenuto, G. Lugones, Strange matter equation of state in the quark mass density dependent model. Phys. Rev. D **51**, 1989 (1995). doi:10.1103/PhysRevD.51.1989

[10] G.X. Peng, H.C. Chiang, J.J. Yang, et al., Mass formulas and thermodynamic treatment in the mass-density-dependent model of strange quark matter. Phys. Rev. C **61**, 015201 (1999). doi:10.1103/PhysRevC.61.015201

[11] G.X. Peng, H.C. Chiang, B.S. Zou, et al., Thermodynamics, strange quark matter, and strange stars. Phys. Rev. C **62**, 025801 (2000). doi:10.1103/PhysRevC.62.025801

[12] R.X. Xu, Solid Quark Stars?. Astrophys. J. Lett. **596**, L59 (2003). doi:10.1086/379209

[13] R.X. Xu, Can cold quark matter be solid? Int. J. Mod. Phys. D **19**, 1437 (2010). doi:10.1142/S0218271810017767

[14] A. Peshier, B. Kmpfer, O. Pavlenko, et al., An effective model of the quark-gluon plasma with thermal parton masses. Phys. Lett. B **337**, 235 (1994). doi:10.1016/0370-2693(94)90969-5

[15] M. Bluhm, B. Kmpfer, G. Soff, The QCD equation of state near T(c) within a quasi-particle model. Phys. Lett. B **620**, 131 (2005). doi:10.1016/j.physletb.2005.05.083

[16] V.M. Bannur, Self-consistent quasiparticle model for quark-gluon plasma. Phys. Rev. C **75**, 044905 (2007). doi:10.1103/PhysRevC.75.044905

[17] F. Gardim, F. Steffens, Thermodynamics of quasi-particles at finite chemical potential. Nucl. Phys. A **825**, 222 (2009). doi:10.1016/j.nuclphysa.2009.05.001

[18] X.J. Wen, Z.Q. Feng, N. Li, et al., Strange quark matter and strangelets in the quasiparticle model. J. Phys. G **36**, 025011 (2009). doi:10.1088/0954-3899/36/2/025011

[19] T. Xia, L. He, P. Zhuang, Three-flavor Nambu–Jona-Lasinio model at finite isospin chemical potential. Phys. Rev. D **88**, 056013 (2013). doi:10.1103/PhysRevD.88.056013

[20] J.-F. Xu, Bulk viscosity of interacting magnetized strange quark matter. Nucl. Sci. Tech. **32**, 111 (2021). doi:10.1007/s41365-021-00954-3

[21] C. Peng, G.-X. Peng, C.-J. Xia, et al., Magnetized strange quark matter in the equivparticle model with both confinement and perturbative interactions. Nucl. Sci. Tech. **27**, 98 (2016). doi:10.1007/s41365-016-0095-5

[22] L. Luo, J. Cao, Y. Yan, et al., A thermodynamically consistent quasi-particle model without density-dependent infinity of the vacuum zero-point energy. Euro. Phys. J. C **73**, 2626 (2013). doi:10.1140/epjc/s10052-013-2626-0

[23] C.J. Xia, G.X. Peng, S.W. Chen, et al., Thermodynamic consistency, quark mass scaling, and properties of strange matter. Phys. Rev. D **89**, 105027 (2014). doi:10.1103/PhysRevD.89.105027

[24] J.F. Xu, G.X. Peng, F. Liu, et al., Strange matter and strange stars in a thermodynamically self-consistent perturbation model with running coupling and running strange quark mass. Phys. Rev. D **92**, 025025 (2015). doi:10.1103/PhysRevD.92.025025

[25] Z.-Y. Lu, G.-X. Peng, S.-P. Zhang, et al., Quark mass scaling and properties of light-quark matter. Nucl. Sci. Tech. **27**, 148 (2016). doi:10.1007/s41365-016-0148-9

[26] P. Demorest, T. Pennucci, S. Ransom, et al., Shapiro delay measurement of a two solar mass neutron star. Nature **467**, 1081 (2010). doi:10.1038/nature09466

[27] E. Fonseca, T.T. Pennucci, J.A. Ellis, et al., The NANOGrav nine-year data set: mass and geometric measurements of binary millisecond pulsars. Astrophys. J. **832**, 167 (2016). doi:10.3847/0004-637X/832/2/167

[28] J. Antoniadis, P.C.C. Freire, N. Wex, et al., A massive pulsar in a compact relativistic binary. Science **340**, 1233232 (2013). doi:10.1126/science.1233232

[29] H.T. Cromartie, E. Fonseca, S.M. Ransom, et al., Relativistic Shapiro delay measurements of an extremely massive millisecond pulsar. Nature Astronomy **4**, 72 (2020). doi:10.1038/s41550-019-0880-2

[30] E. Fonseca, H.T. Cromartie, T.T. Pennucci, et al., Refined mass and geometric measurements of the high-mass PSR J0740+6620. Astrophys. J. Lett. **915**, L12 (2021). doi:10.3847/2041-

8213/ac03b8
[31] D. Blaschke, M. Cierniak, Studying the onset of deconfinement with multi-messenger astronomy of neutron stars. Astron. Nachr. **342**, 227 (2021). doi:10.1002/asna.202113909
[32] H. Liu, J. Xu, P.-C. Chu, Symmetry energy effects on the properties of hybrid stars. Phys. Rev. D **105**, 043015 (2022). doi:10.1103/PhysRevD.105.043015
[33] B.P. Abbott, R. Abbott, T.D. Abbott, et al., GW170817: observation of gravitational waves from a binary neutron star inspiral. Phys. Rev. Lett. **119**, 161101 (2017). doi:10.1103/PhysRevLett.119.161101
[34] The LIGO Scientific Collaboration and the Virgo Collaboration, GW190814: gravitational waves from the coalescence of a 23 solar mass black hole with a 2.6 solar mass compact object. Astrophys. J. Lett. **896**, L44 (2020). doi:10.3847/2041-8213/ab960f
[35] C. Drischler, S. Han, J.M. Lattimer, et al., Limiting masses and radii of neutron stars and their implications. Phys. Rev. C **103**, 045808 (2021). doi:10.1103/PhysRevC.103.045808
[36] G.A. Contrera, D. Blaschke, J.P. Carlomagno, et al., Quark-nuclear hybrid equation of state for neutron stars under modern observational constraints. Phys. Rev. C **105**, 045808 (2022). doi:10.1103/PhysRevC.105.045808
[37] M. Cierniak, D. Blaschke, Hybrid neutron stars in the mass-radius diagram. Astrono. Nachr. **342**, 819 (2021). doi:10.1002/asna.202114000
[38] B.P. Abbott, R. Abbott, T.D. Abbott, et al. (The LIGO Scientific Collaboration and the Virgo Collaboration), GW170817: Measurements of Neutron Star Radii and Equation of State. Phys. Rev. Lett. **121**, 161101 (2018). doi:10.1103/PhysRevLett.121.161101
[39] P.G. Krastev, B.-A. Li, Imprints of the nuclear symmetry energy on the tidal deformability of neutron stars. J. Phys. G **46**, 074001 (2019). doi:10.1088/1361-6471/ab1a7a
[40] Z. Carson, A.W. Steiner, K. Yagi, Constraining nuclear matter parameters with GW170817. Phys. Rev. D **99**, 043010 (2019). doi:10.1103/PhysRevD.99.043010
[41] N.-B. Zhang, B.-A. Li, Extracting nuclear symmetry energies at high densities from observations of neutron stars and gravitational waves. Eur. Phys. J. A **55**, 39 (2019). doi:10.1140/epja/i2019-12700-0
[42] S. Thakur, V. Thakur, R. Kumar, et al., Structural properties of rotating hybrid compact stars with color-flavor-locked quark matter core and their tidal deformability. Eur. Phys. J. A **58**, 93 (2022). doi:10.1140/epja/s10050-022-00744-4
[43] L. Liu, M. Kang, The properties of hybrid stars in a low symmetry energy model. New Astron. 95, 101817 (2022). doi:10.1016/j.newast.2022.101817
[44] H.-M. Jin, C.-J. Xia, T.-T. Sun, et al., arXiv:2205.04801 (2022).
[45] W.-L. Yuan, A. Li, Z. Miao, et al., Interacting ud and uds quark matter at finite densities and quark stars. Phys. Rev. D **105**, 123004 (2022). doi:10.1103/PhysRevD.105.123004
[46] Z.-Q. Miao, C.-J. Xia, X.-Y. Lai, et al., A bag model of matter condensed by the strong interaction. Int. J. Mod. Phys. E **31**, 2250037 (2022). doi:10.1142/S0218301322500379
[47] B. Holdom, J. Ren, C. Zhang, Quark matter may not be strange. Phys. Rev. Lett. **120**, 222001 (2018). doi:10.1103/PhysRevLett.120.222001
[48] L. Wang, J. Hu, C.-J. Xia, et al., Stable up-down quark matter nuggets, quark star crusts, and a new family of white dwarfs. Galaxies **9**, 70 (2021). doi:10.3390/galaxies9040070
[49] G. Pagliara, J. Schaffner-Bielich, Hadron-quark phase transition at nonzero isospin density: The effect of quark pairing. Phys. Rev. D **81**, 094024 (2010). doi:10.1103/PhysRevD.81.094024
[50] G.Y. Shao, M. Colonna, M. Di Toro, et al., Influence of vector interactions on the hadron-quark/gluon phase transition. Phys. Rev. D **85**, 114017 (2012). doi:10.1103/PhysRevD.85.114017
[51] K.S. Jeong, S.H. Lee, Symmetry energy in cold dense matter. Nucl. Phys. A **945**, 21 (2016). doi:10.1016/j.nuclphysa.2015.09.010
[52] L.-W. Chen, Nuclear matter symmetry energy and the symmetry energy coefficient in the mass formula. Phys. Rev. C **83**, 044308 (2011). doi:10.1103/PhysRevC.83.044308
[53] A.W. Steiner, M. Prakash, J.M. Lattimer, et al., Isospin asymmetry in nuclei and neutron stars. Phys. Rept. **411**, 325 (2005). doi:10.1016/j.physrep.2005.02.004
[54] M.Di Toro, B. Liu, V. Greco, et al., Symmetry energy effects on the mixed hadron-quark phase at high baryon density. Phys. Rev. C **83**, 014911 (2011). doi:10.1103/PhysRevC.83.014911
[55] S.-W. Chen, L. Gao, G.-X. Peng, One-gluon-exchange effect on the properties of quark matter and strange stars. Chin. Phys. C **36**, 947 (2012). doi:10.1088/1674-1137/36/10/005
[56] P.-C. Chu, L.-W. Chen, Quark matter symmetry energy and quark stars. Astrophys. J. **780**, 135 (2014). doi:10.1088/0004-637X/780/2/135
[57] L.-W. Chen, Symmetry Energy in Nucleon and Quark Matter. Nucl. Phys. Rev. **34**, 20 (2017). doi:10.11804/NuclPhysRev.34.01.020
[58] T. Damour, A. Nagar, Relativistic tidal properties of neutron stars. Phys. Rev. D **80**, 084035 (2009). doi:10.1103/PhysRevD.80.084035
[59] T. Hinderer, B.D. Lackey, R.N. Lang, et al., Tidal deformability of neutron stars with realistic equations of state and their gravitational wave signatures in binary inspiral. Phys. Rev. D **81**, 123016 (2010). doi:10.1103/PhysRevD.81.123016
[60] S. Postnikov, M. Prakash, J.M. Lattimer, Tidal Love numbers of neutron and self-bound quark stars. Phys. Rev. D **82**, 024016 (2010). doi:10.1103/PhysRevD.82.024016
[61] E.-P. Zhou, X. Zhou, A. Li, Constraints on interquark interaction parameters with GW170817 in a binary strange star scenario. Phys. Rev. D **97**, 083015 (2018). doi:10.1103/PhysRevD.97.083015
[62] L.-W. Chen, C.M. Ko, B.-A. Li, Determination of the stiffness of the nuclear symmetry energy from isospin diffusion. Phys. Rev. Lett. **94**, 032701 (2005). doi:10.1103/PhysRevLett.94.032701
[63] Y. Zhou, L.-W. Chen, Ruling out the supersoft high-density symmetry energy from the discovery of PSR J0740+6620 with mass $2.14^{+0.10}_{-0.09}M_{\odot}$. Astrophys. J. **886**, 52 (2019). doi:10.3847/1538-4357/ab4adf